THE JOURNAL OF PHYSICAL CHEMISTRY LETTERS
A JOURNAL OF THE AMERICAN CHEMICAL SOCIETY

pubs.acs.org/JPCL

Letter

High-Pressure Phase Diagram of the Ti–O System

Kun Li, Junjie Wang,* and Artem R. Oganov*

Cite This: J. Phys. Chem. Lett. 2021, 12, 5486–5493

Read Online

ACCESS | Metrics & More | Article Recommendations | Supporting Information

ABSTRACT: Titanium oxides are technologically important compounds. The chemistry of the Ti–O system is quite rich, largely because of the multiple oxidation states that titanium atoms can take. In this work, using a combination of variable-composition evolutionary crystal structure prediction (USPEX code) and data mining (Materials Project), we predicted all of the stable titanium oxides in the pressure range 0–200 GPa and found that 27 compounds can be stable at different pressures. We resolved contradictions between previous works and predicted four hitherto-unknown stable phases: $P2_1/c$-TiO_3, $I4/mmm$-Ti_3O_2, $Imm2$-Ti_5O_2, and $R\bar{3}$-$Ti_{12}O_5$. We also showed that the high-pressure $P\bar{6}m2$-TiO phase is an electride.

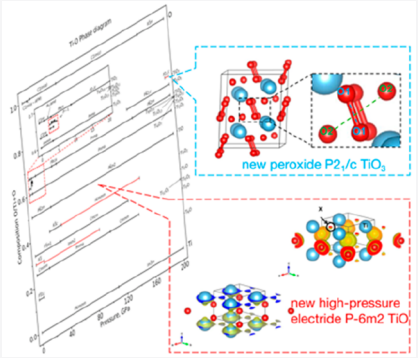

Titanium is the ninth most abundant element in the Earth's crust, where it occurs mainly in oxides and silicates. Like many transition metals, it has multiple oxidation states because of the partially filled 3d shell. The binary Ti–O system has a rich variety of stable stoichiometries, such as Ti_2O, Ti_6O, Ti_3O, and Ti_4O_7.[1−4] Titanium oxides have low toxicity[5] and a number of unique properties, including photocatalytic[6] and catalytic[7] activity, and can also be used in solar cells.[8] Thin films of Ti_2O_3 display superconductivity,[9] and a high-pressure polymorph of TiO_2 was claimed to be an exceptionally hard material[10] (although later this was refuted[11]). Both the stoichiometry and crystal structures of T–O compounds have a strong link to the properties. For example, TiO has metallic conductivity,[12] and TiO_2 polymorphs are semiconductors.[13] Moreover, because of their different crystal structures, TiO_2 polymorphs have different properties: dark-red rutile TiO_2 has a band gap of 3.0 eV and excellent photocatalytic properties, whereas colorless anatase TiO_2 has a wider band gap of 3.2 eV and almost no photocatalytic activity.[13] Recently, superconductivity with T_c = 8 K has been found in Ti^{3+}-based compounds with the electron configuration $3d^1$ in the newly discovered orthorhombic phase of Ti_2O_3 rather than the well-known corundum structure.[9]

The stoichiometry and crystal structure of stable oxides can be tuned by factors such as the temperature, pressure, and oxygen fugacity.[14−19] The influence of temperature on the Ti–O system has been widely investigated. In 1987, using experimental data, Murray and Wriedt[14] published the temperature–composition phase diagram, which showed great richness of titanium oxides with different stoichiometries between pure Ti and TiO_2. Extensive theoretical studies of this phase diagram have also been carried out.[15−19] Moreover, the external pressure can greatly alter the stability and electronic structure of compounds,[20−22] often stabilizing compounds with unusual stoichiometries,[23] structures, and properties[15,16,24,25] and one expects novel titanium oxides to appear. However, most studies of the Ti–O system under pressure have been limited to TiO_2,[10,19,26−33] and the following sequence of phases with increasing pressure was established at pressures up to 200 GPa: rutile ($P4_2/mnm$) or anatase ($I4_1/amd$) → α-PbO_2-type phase ($Pbcn$) → baddeleyite-type "MI" phase ($P2_1/c$) → orthorhombic OI ($Pbca$) → cotunnite-type phase ($Pnma$) → Fe_2P-type phase ($P\bar{6}2m$).

Recently, the new compounds Ti_2O_5 and TiO_3 were predicted to exist at high pressures by Zhong et al.,[16] but the well-known compound Ti_4O_7 was missing on their phase diagram, throwing doubts on their predictions. One possible reason why Ti_4O_7 was missed in that study is that the variable-composition search, a crucial method for predicting new compounds, was not used.[34,35] To test our hypothesis and obtain a more accurate pressure–composition phase diagram of the Ti–O system, we employed the variable-composition search algorithm USPEX (Universal Structure Predictor: Evolutionary Xtallography)[36−39] to search for structures with global stability at pressures in the range 0–200 GPa and predicted four new stable phases. Then, on the basis of the 115 structures predicted in this study and those derived from the Materials Project database[40] and the literature,[15,16,24,25] we drew a new pressure–composition phase diagram of the Ti–O

Received: April 9, 2021
Accepted: June 3, 2021
Published: June 4, 2021

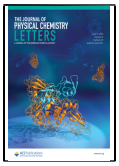

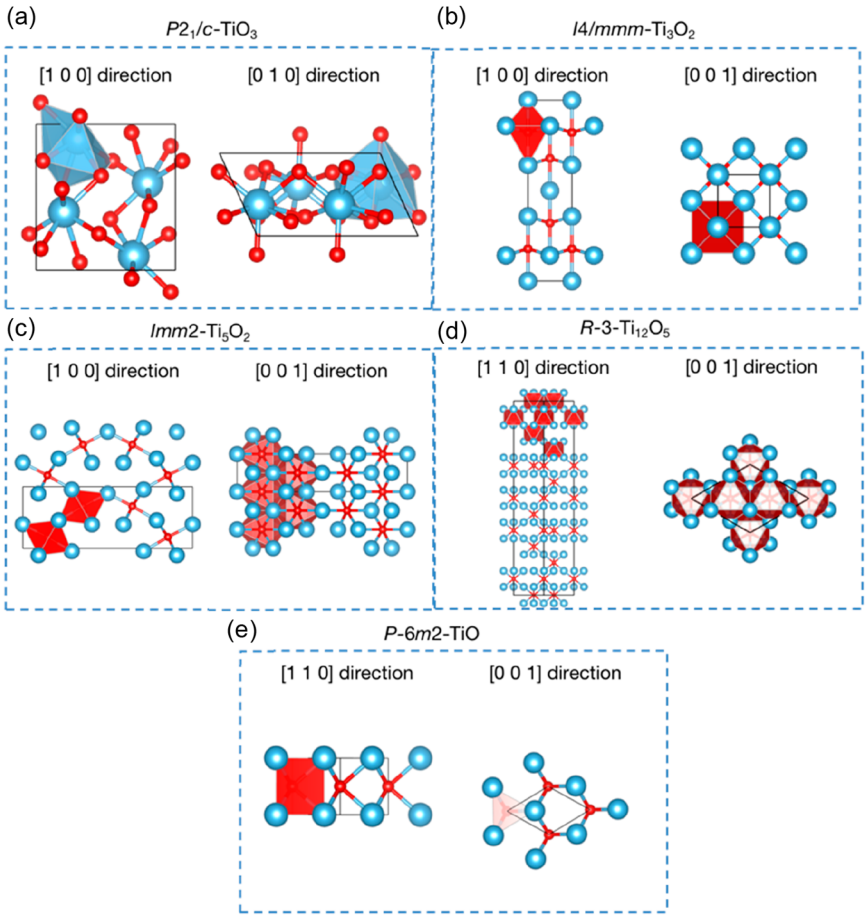

Figure 1. Crystal structures of (a) $P2_1/c$-TiO_3, (b) $I4/mmm$-Ti_3O_2, (c) $Imm2$-Ti_5O_2, (d) $R\bar{3}$-$Ti_{12}O_5$, and (e) $P\bar{6}m2$-TiO shown in different directions. Ti and O atoms are shown as blue and red spheres, respectively.

system. In addition, we found that the structure of TiO_3 predicted in the previous study[16] is unstable and explained why. Finally, we proved that the known high-pressure phase $P\bar{6}m2$-TiO is an electride.

The convex hull diagrams of the Ti−O system in the pressure range 0−200 GPa are shown in Figure S1. The structures lying on the convex hull are thermodynamically stable. Besides the previously reported structures, four new titanium oxides were predicted in our study for the first time: $P2_1/c$-TiO_3, $I4/mmm$-Ti_3O_2, $Imm2$-Ti_5O_2, and $R\bar{3}$-$Ti_{12}O_5$ (Figure 1a−d). In addition, the $P\bar{6}m2$-TiO structure documented in the Materials Project database (Figure 1e) was identified as a high-pressure electride and will be discussed later. Crystal structures of these new structures at pressures of their stability are listed in Table S1, and their phonon dispersion curves are shown in Figure S2. The absence of imaginary frequencies proves their dynamic stability.

On the basis of the convex hull diagrams, a pressure−composition phase diagram of the Ti−O system was drawn (Figure 2). A total of 27 binary Ti−O compounds are present on the phase diagram. The well-known TiO, Ti_2O_3, and TiO_2 compounds are stable over the whole pressure range (Figure 2). None of the Ti-rich compounds Ti_6O, Ti_3O, Ti_5O_2, $Ti_{12}O_5$, and Ti_3O_2 are stable at pressures above 150 GPa (Figure 2). In the composition range from Ti_6O to Ti_3O, only $P\bar{3}1c$-Ti_6O is stable from 0 to 8 GPa and more energetically favorable than Zr_6O/Hf_6O-type ($R\bar{3}$) Ti_6O over the whole pressure range. However, several reported stable Ti-rich phases at high pressure, e.g., $P\bar{1}$-Ti_5O, $C2/m$-Ti_5O, and $Pmmm$-Ti_4O,[15] were found to be above the convex hull, albeit slightly (detailed information is given in Table S3).

At the same time, high pressure promotes the formation of O-rich compounds, as it does in the Zr−O and Hf−O systems. Two O-rich stoichiometries, Ti_2O_5 and TiO_3, successively appear on the phase diagram at pressures above 140 GPa (Figure 2), which is consistent with the previous work.[16] The monoclinic phase $P2_1/c$-TiO_3 (Figure 1a), predicted for the first time in this study, is the most stable TiO_3 phase at pressures around 200 GPa, and the previously predicted[15,16] $Pm\bar{3}n$-TiO_3 structure is unstable. $P2_1/c$-TiO_3 becomes stable at a much higher pressure (195 GPa) than ZrO_3 (80 GPa)[25] and HfO_3 (110 GPa).[24] In this new phase of TiO_3, Ti atoms occupy the Wyckoff position 4*e* (0.382, 0.700, 0.099), whereas O atoms occupy three Wyckoff positions: 4*e* (0.174, 0.548, 0.749), 4*e* (0.225, 0.185, 0.556), and 4*e* (0.232, 0.534, 0.352). The most interesting aspect of the new structure is that it is an "oxide peroxide" and contains both oxide (O^{2-}) and peroxide (O_2^{2-}) ions, and its formula can be written as $TiO[O_2]$—previously, such oxide peroxides as $AlO_2 = Al_4O_4[O_2]_2$ and $Al_4O_7 = Al_4O_5[O_2]$ were predicted to appear at high pressures in the Al−O system.[41] We recall that O−O bond lengths under normal conditions are 1.21 Å in the O_2 molecule, 1.28 Å in the superoxide ion (O_2^-), and 1.47 Å in the peroxide ion. We also relaxed the structure of MgO_2 peroxide at 200 GPa and found

https://doi.org/10.1021/acs.jpclett.1c01133
J. Phys. Chem. Lett. 2021, 12, 5486−5493

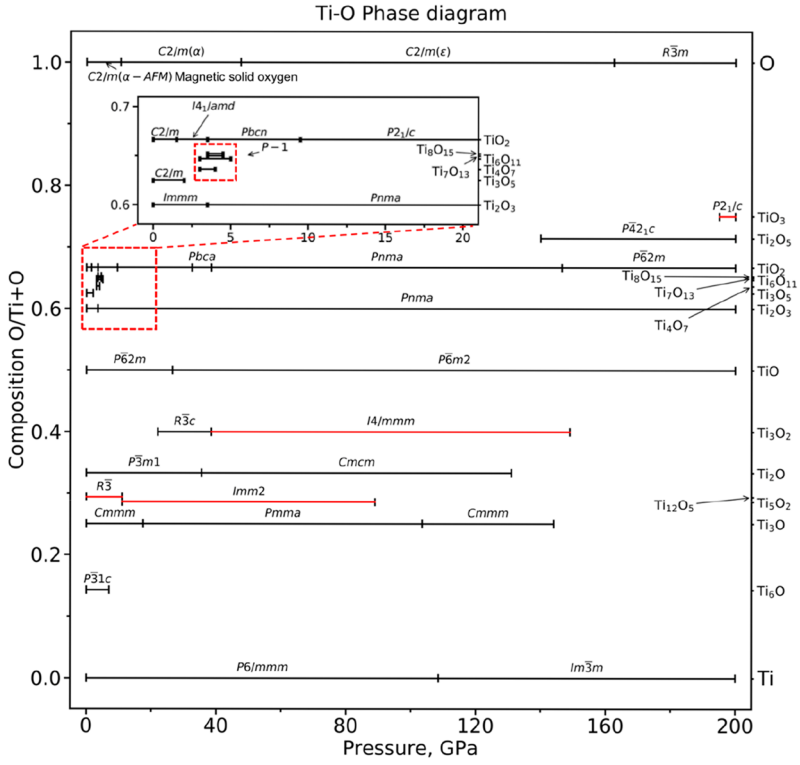

Figure 2. Pressure−composition phase diagram of the Ti−O system. The stable phases predicted in this work and in previous studies are shown by red and black lines, respectively.

the nearest O−O distance to be 1.37 Å, which is comparable to the nearest O−O distance (1.30 Å) at 200 GPa in the crystal structure of the new TiO_3 phase (Figure 1a) and indeed confirmed that this TiO_3 is a peroxide. Later we will discuss what makes this structure more stable than the previously predicted non-peroxide $Pm\bar{3}n$-TiO_3.

Compared with the pressure range of stability of $R\bar{3}c$-Zr_3O_2 (39−72 GPa),[25] the known $R\bar{3}c$-Ti_3O_2 structure[40] undergoes a phase transition to the hitherto-unknown $I4/mmm$-Ti_3O_2 at 38.5 GPa, which remains stable at pressures up to 149 GPa (Figure 2). In this phase, Ti atoms form a bcc sublattice, where O atoms fill some of the octahedral voids, leading to symmetry lowering from cubic to tetragonal (Figure 1b). Similar to $R\bar{3}$-$Zr_{12}O_5$ (0−11 GPa),[25] $R\bar{3}$-$Ti_{12}O_5$ is stable only at low pressure (0−11 GPa). It has oxygen interstitials in the hcp-Ti sublattice, and TiO_6 octahedra share corners and edges (Figure 1d). With a further increase of pressure, a new phase of Ti_5O_2 was found to become stable. This phase has $Imm2$ symmetry, and in its structure each O atom sits at the center of an octahedron formed by six nearest Ti atoms (Figure 1c).

Pressure-induced phase transitions of TiO, an important compound in the Ti−O system, have attracted the interest of researchers.[16,18] For example, Zhong et al.[16] proposed a phase transition sequence $A2/m$-TiO → $Fm\bar{3}m$-TiO (at ∼50 GPa) → $Pm\bar{3}m$-TiO (at ∼75 GPa). However, our calculations completely contradict this picture and reveal that $P\bar{6}2m$-TiO is more stable than $A2/m$-TiO in the low-pressure range 0−26.5 GPa, whereas $P\bar{6}m2$-TiO has the lowest enthalpy in the pressure range from 26.5 to 200 GPa. Interestingly, both $P\bar{6}2m$-type HfO and ZrO were reported in the previous phase diagram, and $P\bar{6}2m$-ZrO was identified as the ground state.[24,25] Our result is consistent with the previous study by Chtchelkatchev et al.,[18] in which the phase transition from ϵ-TiO ($P\bar{6}2m$) to H-TiO ($P\bar{6}m2$) occurred at 28 GPa and $A2/m$-TiO was found to be a metastable phase in the pressure range from 0 to 100 GPa.

Our results for pressure-induced phase transitions of TiO_2 (Figure 2) show excellent agreement with the previous work of Fu et al.[19] Although anatase ($I4_1/amd$) TiO_2 was theoretically[19] believed to be the ground state at 0 GPa (while experimentalists believed that the rutile ($P4_2/mnm$) phase is the ground state at room temperature[42]), we found the β-TiO_2 ($C2/m$) structure[43,44] to have the lowest energy at 0 GPa (Figure 2). β-TiO_2 was first synthesized by the hydrolysis of $K_2Ti_4O_9$[43] and then reported to be a natural polymorph in anatase crystals from Switzerland.[44] The theoretical energy differences are small: the anatase and rutile phases are only 5.9 and 36.6 meV/atom higher in energy than the $C2/m$ one, respectively. With increasing pressure, phase transitions occur at 1.5, 3.5, 9.5, 32.5, 38.5, and 146.5 GPa in the sequence β-TiO_2 ($C2/m$)→ anatase ($I4_1/amd$) → α-PbO_2-type phase ($Pbcn$) → baddeleyite-type "MI" phase ($P2_1/c$) → orthorhombic OI ($Pbca$) → cotunnite-type phase ($Pnma$) → Fe_2P-type phase ($P\bar{6}2m$), which is consistent with the previous work[19] and the Materials Project database.[40] Structural information on all structures used in the construction of the Ti−O phase diagram is provided in the Supporting Information. Table S2 lists the lattice constants and sources of these structures, while Table S3 gives the distances to the convex hull of all phases at 0, 50, 100, 150, and 200 GPa. In addition, the stable pressure of each structure on the phase diagram is listed in Table S4.

To gain further insight, we calculated band structures and densities of states (DOS) of $R\bar{3}$-$Ti_{12}O_5$, $Imm2$-Ti_5O_2, $I4/mmm$-Ti_3O_2, and $P2_1/c$-TiO_3 using density functional theory (Figures 3 and S3). Three Ti-rich structures ($R\bar{3}$-$Ti_{12}O_5$,

https://doi.org/10.1021/acs.jpclett.1c01133
J. Phys. Chem. Lett. 2021, 12, 5486−5493

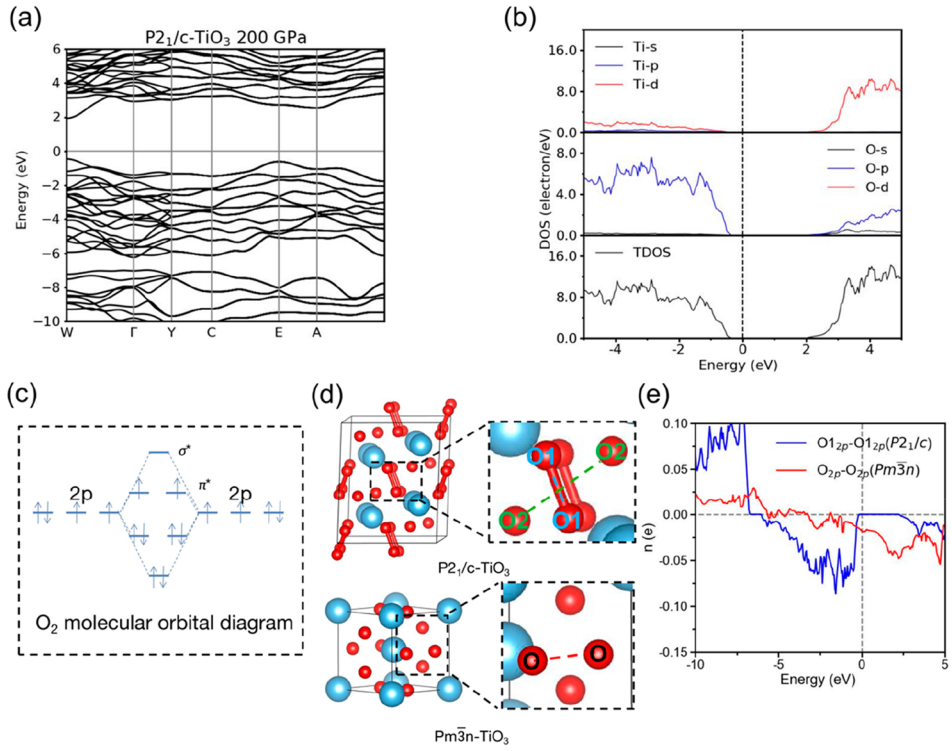

Figure 3. Calculated (a) band structure and (b) density of states of $P2_1/c$-TiO_3. (c) Orbital diagram of molecular O_2. (d) Illustration of the corresponding fragments of the structure and (e) the calculated crystal orbital overlap populations of the O−O pairs in $P2_1/c$-TiO_3 and $Pm\bar{3}n$-TiO_3. All of the calculations were carried out at 200 GPa.

*Imm*2-Ti_5O_2, and *I*4/*mmm*-Ti_3O_2) are metallic, as evidenced by the bands crossing the Fermi level. The DOS calculations show strong peaks of the Ti d orbitals around the Fermi level, implying that the contribution of the Ti d states is responsible for the metallicity of the Ti-rich compounds (Figure S3). The average Bader charges of the Ti atoms for $R\bar{3}$-$Ti_{12}O_5$ (0 GPa), *Imm*2-Ti_5O_2 (50 GPa), and *I*4/*mmm*-Ti_3O_2 (100 GPa) are 0.60*e*, 0.67*e*, and 1.01*e*, respectively.

The O-rich structure $P2_1/c$-TiO_3 is an insulator, possessing a calculated direct band gap of 2.38 eV at the *k* point W(0.5, 0, 0) (Figure 3a). The calculated DOS shows a closed-shell electronic structure (which $TiO[O_2]$ should indeed have) with the valence-band maximum dominated by the O p orbitals, whereas the lowest unoccupied states are predominantly derived from the Ti d orbitals. The calculated Bader charges of the Ti atoms in $P2_1/c$-TiO_3 (200 GPa) are 2.07*e*, which is very close to the value of 2.08*e* in semiconducting $P\bar{6}2m$-TiO_2. Oxygen atoms occupy two different positions: O1 atoms form peroxo ions (the Bader charge of O1 atoms is −0.53*e*), whereas O2 atoms are oxide ions (the Bader charge is −1.01*e*, which can be compared with the Bader charge of −1.04*e* for oxygen in $P\bar{6}2m$-TiO_2). In addition, the projected density of states of these O atoms in $P2_1/c$ and $Pm\bar{3}n$ TiO_3 is shown in Figure S3. From the plot, we can see that the O2 p orbital makes the highest contribution to the total DOS below the Fermi level, while O p ($Pm\bar{3}n$) makes a lower contribution and O1 p makes the lowest. Notably, among these three orbitals, only O p ($Pm\bar{3}n$) is an unfilled orbital in the energy range from 0 to 2 eV, from which it can be understood that the O2 p orbital is fully occupied and O1 atoms bond with each other by covalent bonds to form a closed-shell structure. Therefore, one can conclude that O1−O1 can be regarded as O_2^{2-} and that O2 is O^{2-}.

Our newly predicted $P2_1/c$-TiO_3 is more stable than the previously predicted[16] $Pm\bar{3}n$-TiO_3 structure over the entire pressure range studied here (Figure S4). $Pm\bar{3}n$-TiO_3 is a metallic phase (Figure S3) and has a highly symmetric structure with the nearest O−O distances equal to 1.76 Å. In contrast, $P2_1/c$-TiO_3 is an insulating phase with broken symmetry due to the formation of a strongly bound O−O pair, which we identified as the peroxide ion. Such symmetry breaking and band gap opening are signs of electronic stabilization of the structure. Figure 3c shows the molecular orbital diagram of the O_2 molecule, with two half-filled antibonding π^* orbitals and an empty antibonding σ^* orbital. Attracting two electrons, the O_2 molecule puts them in the π^* orbitals and becomes the closed-shell nonmagnetic peroxide ion O_2^{2-}; occupation of antibonding levels weakens the O−O bond and makes it longer. In both the $P2_1/c$ and $Pm\bar{3}n$ structures, titanium is in the Ti^{4+} oxidation state, and its valence is fully satisfied by oxygen; the difference is mainly in the oxygen sublattice. The stability of the symmetry-broken insulating $P2_1/c$ phase versus the high-symmetry metallic $Pm\bar{3}n$ phase of TiO_3 can be viewed as a result of a Peierls distortion: symmetry breaking (leading to pairing of some oxygens to form the closed-shell O_2^{2-} ions) lowers the electronic energy and can be overturned by the *PV* term in the free energy only at very high pressures (~250 GPa; see Figure S4). In addition, previous studies have shown that the peroxide structure is energetically preferred in O-rich compounds, e.g., in ZrO_3 and HfO_3, and this peroxide structure is the main difference between $Pm\bar{3}n$-TiO_3 and $P2_1/c$-TiO_3. Therefore, it is highly possible that the peroxide structure is a key factor in the high stability of the $P2_1/c$ phase.

In the structures of $P2_1/c$-TiO_3 and $Pm\bar{3}n$-TiO_3, we see nearest O−O distances equal to 1.30, 2.33, and 2.07 for O1−

https://doi.org/10.1021/acs.jpclett.1c01133
J. Phys. Chem. Lett. 2021, 12, 5486−5493

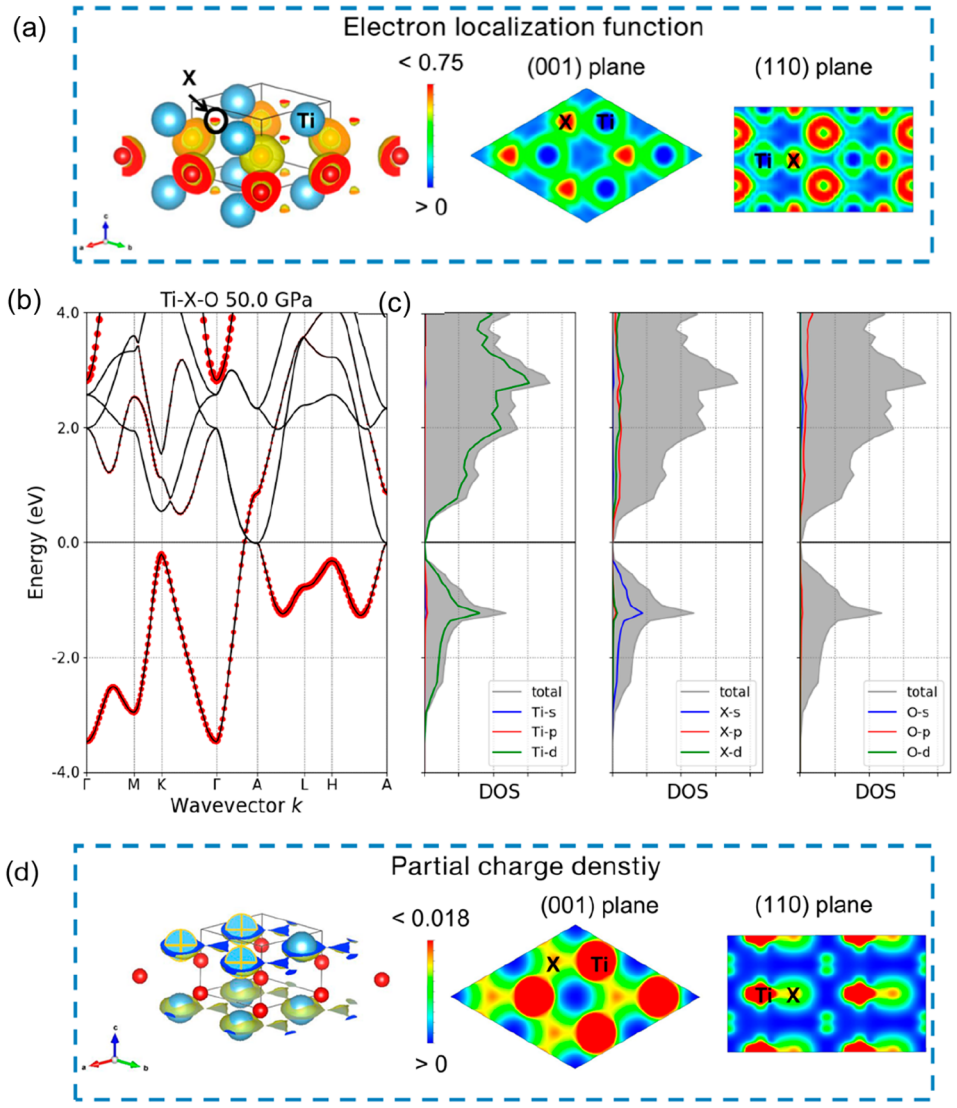

Figure 4. Electronic structure of $P\bar{6}m2$-TiO at 50 GPa. (a) ELF of $P\bar{6}m2$-TiO at 50 GPa with the isosurface at ELF = 0.75. (b) Calculated projected band structure, with the contribution of electrons at the interstitial sites indicated by red dots, and (c) DOS of $P\bar{6}m2$-TiO at 50 GPa. (d) Partial charge density with the isosurface at 0.014 e/Å^3 below the Fermi level (E_F) (-1 eV $< E - E_F <$ 0 eV)

O1, O2−O2, O1−O2 in $P2_1/c$-TiO_3 and 1.76 Å for O−O in $Pm\bar{3}n$-TiO_3 (Figure 3d). Significant orbital overlap can be expected only in O1−O1 and possibly O−O ($Pm\bar{3}n$-TiO_3) interactions, for which we calculated the crystal orbital overlap populations (COOPs). Positive and negative values of COOP correspond to bonding and antibonding states, respectively. The calculated COOP values for the O1− O1 interactions in $P2_1/c$-TiO_3 (Figure 3e) show antibonding due to $O1_{2p}$−$O1_{2p}$ interactions in the energy range from −6 to 0 eV (and bonding interactions at lower energies). In contrast, the O_{2p}−O_{2p} interaction in $Pm\bar{3}n$-TiO_3 leads to strong antibonding states at around 0 eV, indicating unfilled orbitals with high energy. In addition, the negative integrated crystal orbital Hamilton population (−ICOHP) values shown in Table S5 indicate that O−O bonding is stronger in $P2_1/c$ than in $Pm\bar{3}n$-TiO_3. From the COOP analysis, we can infer that in the $P2_1/c$ phase the O1−O1 π^* orbital is fully occupied, which indicates that the O1−O1 group can be regarded as O_2^{2-}. On the contrary, the O−O σ^* orbital is partially occupied in $Pm\bar{3}n$-TiO_3, and the O−O bond is not thoroughly broken, which is physically unfavorable and would lower the stability of TiO_3.

Electrides are a class of exotic materials that are promising as electron emitters,[45] catalysts,[46,47] etc. In these materials, the highly localized electrons in voids of the structure can act as anions and lead to a very low work function. Because electrides generally exist in electron-rich systems, Ti-rich compounds such as TiO, Ti_2O, and Ti_5O_2 have the potential to belong to in this class. Actually, Zhong et al.[15] suggested that Ti_2O could be an electride. In this work, we found that $P\bar{6}m2$-TiO, a high-pressure phase, is a new electride in the Ti−O system.

The calculated electron localization function (ELF) of $P\bar{6}m2$-TiO has a maximum (labeled X) at the center of the triangle composed of three Ti atoms, which suggests that this phase might be described as an electride (Figure 4a). To correctly identify the contribution of the interstitial electrons to bands of $P\bar{6}m2$-TiO, we placed pseudoatoms at X sites with the integration radius of 1.5 Å and computed the projected band structure and partial density of states for the electrons from the interstitial X sites (Figure 4b,c). The projected band

https://doi.org/10.1021/acs.jpclett.1c01133
J. Phys. Chem. Lett. 2021, 12, 5486−5493

structure shows a single and dispersive band (interstitial band) below the Fermi level (E_F) (-4 eV < $E - E_F$ < 0 eV) that is significantly affected by the electrons in interstitial X regions (red dots in Figure 4b). The DOS calculations also show a large contribution of the interstitial electrons to the states below the Fermi level (Figure 4c). To visualize the real-space distribution of electrons around the Fermi level, the decomposed partial charge density was calculated in the range of -1 eV < $E - E_F$ < 0 eV (Figure 4d). The calculation result shows that the states below the Fermi level are partially localized at the interstitial X sites. The formation of the electride is likely related to the pressure-enhanced multicenter orbital overlap between the Ti d orbitals.[48,49] Moreover, the interstitial electrons could form an ionic interaction with the Ti atoms, leading to structural stabilization. Although the stability of $P\bar{6}m2$-TiO at high pressures has been studied before,[18] this is the first time that the electride nature of this compound was identified. We also checked the electronic structures of $R\bar{3}$-$Ti_{12}O_5$, $I4/mmm$-Ti_3O_2, $R\bar{3}c$-Ti_3O_2, and $Imm2$-Ti_5O_2. From the ELF plots, there are no localized electrons in the interstitials of $Ti_{12}O_5$ and the two Ti_3O_2 structures (Figure S5), which indicates that they are not electrides. Interestingly, a sign of localized electrons was found in the interstitial position of $Imm2$-Ti_5O_2 at 50 GPa (Figure S6). However, detailed analysis showed that the energy level of the localized electrons stays away from the Fermi level and makes a greater contribution to the energy level range from -1.5 to 0.5 eV, which means that the feature of electrides in $Imm2$-Ti_5O_2 is weak (Figure S6). Therefore, $Imm2$-Ti_5O_2 at 50 GPa cannot be regarded as an electride either.

In this work, we performed a systematic investigation of the stability of Ti−O compounds at pressures up to 200 GPa and constructed an accurate pressure−composition phase diagram. Twenty-seven phases have stability fields on this phase diagram, including four new stable Ti−O compounds: $P2_1/c$-TiO_3, $I4/mmm$-Ti_2O_3, $Imm2$-Ti_5O_2, and $R\bar{3}$-$Ti_{12}O_5$. The comparison of the electronic structures of our newly predicted $P2_1/c$-TiO_3 and the previously predicted $Pm\bar{3}n$-TiO_3 reveals Peierls distortion as the reason why the former structure is stable in the studied pressure range while the latter one is not. In addition, the $P2_1/c$ phase is found to be an oxide peroxide, $TiO[O_2]$. We have also shown that the previously predicted phase $P\bar{6}m2$-TiO is a high-pressure electride. The Ti−O system is one of the more studied chemical systems, yet the application of pressure brings about many unexpected compounds and crystal structures with interesting aspects of chemical bonding and physical properties. Clearly, high pressure is a powerful route to alter the chemical behavior of elements and compounds.

COMPUTATIONAL METHODS

In this work, stable compounds in the Ti−O system were searched at 0, 50, 100, 150, and 200 GPa using a combination of the evolutionary structure prediction algorithm USPEX[36−39] with first-principles calculations done using the Vienna Ab Initio Simulation Package (VASP).[50] Variable-composition search allowed all Ti_xO_y compositions under the constraint of fewer than 16 atoms in the primitive cell. Global optimization was performed using USPEX, a powerful tool for predicting novel unknown materials that has successfully found many new crystalline phases of various materials,[51−54] in particular under extreme conditions.[22,23,55,56] All of the structures of the first generation were produced using the random symmetric structure generator[39] and were relaxed using VASP, and the first convex hull was built on the basis of the enthalpies of the relaxed structures. Structures closest to the convex hull were used as parents for the generation of new structures, which were also relaxed, leading to an updated convex hull, after which the next generation of structures was found, and so on. Each new generation was produced from the previous generation using heredity (50%), lattice mutation (20%), and transmutation (10%) operators; 20% of the structures of each new generation were produced by the random symmetric generator. Each search continued for 30 generations.

Structure relaxation was done with the VASP code using the projector augmented wave (PAW) method[57] to describe the interactions between the ions and electrons (with [Ar] and [He] cores for Ti and O atoms, respectively), whereas the exchange−correlation interaction between the electrons was modeled using the generalized gradient approximation (GGA) with the Perdew−Burke−Ernzerhof (PBE) functional.[58] Structure relaxation proceeded until changes in the enthalpy were below 10^{-4} eV/cell and the forces on each atom became smaller than 0.01 eV/Å. In these calculations, a plane-wave kinetic energy cutoff of 550 eV and uniform k-point meshes with reciprocal-space resolution of $2\pi \times 0.03$ Å^{-1} were used.

For the predicted stable structures, we used a cutoff energy of 600 eV and a k-point grid resolution of $2\pi \times 0.02$ Å^{-1} for further structure relaxation and electronic structure calculations. These more precise relaxations terminated when the forces on atoms were below 0.005 eV/Å. The resulting enthalpies thus obtained were used to construct accurate Ti−O convex hulls at different pressures and pressure−composition phase diagrams. The enthalpy of formation of Ti−O compounds was calculated using the following formula:

$$\Delta H_f = \frac{H(Ti_xO_y) - [xH(Ti) + yH(O)]}{x + y} \quad (1)$$

where $H(Ti_xO_y)$ is the calculated enthalpy of the Ti−O compound, H(Ti) and H(O) are the enthalpies of Ti and O in their stable states at the given pressure, respectively, and x and y are the stoichiometric proportions of Ti and O in the Ti−O compound, respectively. To check the dynamic stability of the predicted structures, phonon dispersions were calculated by employing the finite displacement method as implemented in the Phonopy code.[59]

To further study the electronic properties, we calculated the net charges of atoms using Bader analysis of the total electron density.[60] In addition, the crystal orbital overlap populations (COOPs) were examined by LOBSTER[61] to analyze chemical bonding in the predicted titanium oxides.

ASSOCIATED CONTENT

Supporting Information

The Supporting Information is available free of charge at https://pubs.acs.org/doi/10.1021/acs.jpclett.1c01133.

Convex hull diagrams of the Ti−O system at different pressures, calculated phonon dispersions and electronic structures of newly found Ti−O structures at different pressures, enthalpies of TiO_3 and Ti_3O phases as functions of pressure, structural parameters of the predicted Ti−O compounds at pressures of their stability, calculated ELFs of Ti−O compounds, and structural parameters and sources of the Ti−O compounds (PDF)

https://doi.org/10.1021/acs.jpclett.1c01133
J. Phys. Chem. Lett. 2021, 12, 5486−5493

AUTHOR INFORMATION

Corresponding Authors

Junjie Wang − *State Key Laboratory of Solidification Processing, Northwestern Polytechnical University, Xi'an, Shaanxi 710072, People's Republic of China;* orcid.org/0000-0002-6428-2233; Email: wang.junjie@nwpu.edu.cn

Artem R. Oganov − *Skolkovo Institute of Science and Technology, Moscow 143026, Russia;* orcid.org/0000-0001-7082-9728; Email: A.Oganov@skoltech.ru

Author

Kun Li − *State Key Laboratory of Solidification Processing, Northwestern Polytechnical University, Xi'an, Shaanxi 710072, People's Republic of China*

Complete contact information is available at: https://pubs.acs.org/10.1021/acs.jpclett.1c01133

Notes

The authors declare no competing financial interest.

ACKNOWLEDGMENTS

This work was supported by the National Natural Science Foundation of China (Grant 51872242, 52111530033) and the Fundamental Research Funds for the Central Universities (D5000200142). A.R.O. thanks the Russian Ministry of Science and Higher Education (Grant 2711.2020.2 to leading scientific schools).

REFERENCES

(1) Yamaguchi, S.; Koiwa, M.; Hirabayashi, M. Interstitial Superlattice of Ti_6O and Its Transformation. *J. Phys. Soc. Jpn.* **1966**, *21*, 2096.

(2) Jostsons, A.; Malin, A. S. The Ordered Structure of Ti_3O. *Acta Crystallogr., Sect. B: Struct. Crystallogr. Cryst. Chem.* **1968**, *24*, 211−213.

(3) Le Page, Y.; Marezio, M. Structural Chemistry of Magnéli Phases $TinO_{2n-1}$ ($4 \leq n \leq 9$): IV. Superstructure in Ti_4O_7 at 140 K. *J. Solid State Chem.* **1984**, *53*, 13−21.

(4) Novoselova, T.; Malinov, S.; Sha, W.; Zhecheva, A. High-Temperature Synchrotron X-Ray Diffraction Study of Phases in a Gamma TiAl Alloy. *Mater. Sci. Eng., A* **2004**, *371*, 103−112.

(5) Pan, X.; Yang, M. Q.; Fu, X.; Zhang, N.; Xu, Y. J. Defective TiO_2 with Oxygen Vacancies: Synthesis, Properties and Photocatalytic Applications. *Nanoscale* **2013**, *5*, 3601−3614.

(6) Schneider, J.; Matsuoka, M.; Takeuchi, M.; Zhang, J.; Horiuchi, Y.; Anpo, M.; Bahnemann, D. W. Understanding TiO_2 Photocatalysis: Mechanisms and Materials. *Chem. Rev.* **2014**, *114*, 9919−9986.

(7) Hadjiivanov, K. I.; Klissurski, D. G. Surface Chemistry of Titania (Anatase) and Titania-Supported Catalysts. *Chem. Soc. Rev.* **1996**, *25*, 61−69.

(8) O'Regan, B.; Grätzel, M. High-Efficiency Solar Cell Based on Dye-Sensitized Colloidal TiO_2 Films. *Nature* **1991**, *353*, 737−740.

(9) Li, Y.; Weng, Y.; Zhang, J.; Ding, J.; Zhu, Y.; Wang, Q.; Yang, Y.; Cheng, Y.; Zhang, Q.; Li, P.; et al. Observation of Superconductivity in Structure-Selected Ti_2O_3 Thin Films. *NPG Asia Mater.* **2018**, *10*, 522−532.

(10) Dubrovinsky, L. S.; Dubrovinskaia, N. A.; Swamy, V.; Muscat, J.; Harrison, N. M.; Ahuja, R.; Holm, B.; Johansson, B. The Hardest Known Oxide. *Nature* **2001**, *410*, 653−654.

(11) Lyakhov, A. O.; Oganov, A. R. Evolutionary Search for Superhard Materials: Methodology and Applications to Forms of Carbon and TiO_2. *Phys. Rev. B: Condens. Matter Mater. Phys.* **2011**, *84*, 092103.

(12) Bartkowski, S.; Neumann, M.; Kurmaev, E. Z.; Fedorenko, V. V.; Shamin, S. N.; Cherkashenko, V. M.; Nemnonov, S. N.; Winiarski, A.; Rubie, D. C. Electronic Structure of Titanium Monoxide. *Phys. Rev. B: Condens. Matter Mater. Phys.* **1997**, *56*, 10656−10667.

(13) Hashimoto, K.; Irie, H.; Fujishima, A. TiO_2 Photocatalysis: A Historical Overview and Future Prospects. *Jpn. J. Appl. Phys.* **2005**, *44*, 8269−8285.

(14) Murray, J. L.; Wriedt, H. A. The O−Ti (Oxygen−Titanium) System. *J. Phase Equilib.* **1987**, *8*, 148−165.

(15) Zhong, X.; Xu, M.; Yang, L.; Qu, X.; Yang, L.; Zhang, M.; Liu, H.; Ma, Y. Predicting the Structure and Stability of Titanium Oxide Electrides. *npj Comput. Mater.* **2018**, *4*, 70.

(16) Zhong, X.; Yang, L.; Qu, X.; Wang, Y.; Yang, J.; Ma, Y. Crystal Structures and Electronic Properties of Oxygen-rich Titanium Oxides at High Pressure. *Inorg. Chem.* **2018**, *57*, 3254−3260.

(17) Gunda, N. S. H.; Puchala, B.; Van der Ven, A. Resolving Phase Stability in the Ti-O Binary with First-principles Statistical Mechanics Methods. *Phys. Rev. Mater.* **2018**, *2*, 033604.

(18) Chtchelkatchev, N. M.; Ryltsev, R. E.; Kostenko, M. G.; Rempel, A. A. Stability of Defectless Structures of Titanium Monoxide at High Pressures. *JETP Lett.* **2018**, *108*, 476−480.

(19) Fu, Z.; Liang, Y.; Wang, S.; Zhong, Z. Structural Phase Transition and Mechanical Properties of TiO_2 under High Pressure. *Phys. Status Solidi B* **2013**, *250*, 2206−2214.

(20) Miao, M.; Wang, X.; Brgoch, J.; Spera, F.; Jackson, M. G.; Kresse, G.; Lin, H. Anionic Chemistry of Noble Gases: Formation of Mg-NG (NG = Xe, Kr, Ar) Compounds under Pressure. *J. Am. Chem. Soc.* **2015**, *137*, 14122−14128.

(21) Miao, M.; Hoffmann, R. High Pressure Electrides: A Predictive Chemical and Physical Theory. *Acc. Chem. Res.* **2014**, *47*, 1311−1317.

(22) Dong, X.; Oganov, A. R.; Goncharov, A. F.; Stavrou, E.; Lobanov, S.; Saleh, G.; Qian, G.-R.; Zhu, Q.; Gatti, C.; Deringer, V. L.; et al. A Stable Compound of Helium and Sodium at High Pressure. *Nat. Chem.* **2017**, *9*, 440−445.

(23) Zhang, W.; Oganov, A. R.; Goncharov, A. F.; Zhu, Q.; Boulfelfel, S. E.; Lyakhov, A. O.; Stavrou, E.; Somayazulu, M.; Prakapenka, V. B.; Konôpková, Z. Unexpected Stable Stoichiometries of Sodium Chlorides. *Science* **2013**, *342*, 1502−1505.

(24) Zhang, J.; Oganov, A. R.; Li, X.; Xue, K.; Wang, Z.; Dong, H. Pressure-induced Novel Compounds in the Hf-O System from First-principles Calculations. *Phys. Rev. B: Condens. Matter Mater. Phys.* **2015**, *92*, 184104.

(25) Zhang, J.; Oganov, A. R.; Li, X.; Mahdi Davari Esfahani, M.; Dong, H. First-Principles Investigation of Zr-O Compounds, Their Crystal Structures, and Mechanical Properties. *J. Appl. Phys.* **2017**, *121*, 155104.

(26) Ma, X. G.; Liang, P.; Miao, L.; Bie, S. W.; Zhang, C. K.; Xu, L.; Jiang, J. J. Pressure-Induced Phase Transition and Elastic Properties of TiO_2 Polymorphs of TiO_2 Polymorphs. *Phys. Status Solidi B* **2009**, *246*, 2132−2139.

(27) Dubrovinskaia, N. A.; Dubrovinsky, L. S.; Ahuja, R.; Prokopenko, V. B.; Dmitriev, V.; Weber, H. P.; Osorio-Guillen, J. M.; Johansson, B. Experimental and Theoretical Identification of a New High-pressure TiO_2 Polymorph. *Phys. Rev. Lett.* **2001**, *87*, 275501.

(28) Swamy, V.; Muddle, B. C. Ultrastiff Cubic TiO_2 Identified via First-principles Calculations. *Phys. Rev. Lett.* **2007**, *98*, 035502.

(29) Sato, H.; Endo, S.; Sugiyama, M.; Kikegawa, T.; Shimomura, O.; Kusaba, K. Baddeleyite-type High-pressure Phase of TiO_2. *Science* **1991**, *251*, 786−788.

(30) Muscat, J.; Swamy, V.; Harrison, N. M. First-Principles Calculations of the Phase Stability of TiO_2. *Phys. Rev. B: Condens. Matter Mater. Phys.* **2002**, *65*, 224112.

(31) Lagarec, K.; Desgreniers, S. Raman Study of Single Crystal Anatase TiO_2 up to 70 GPa. *Solid State Commun.* **1995**, *94*, 519−524.

(32) Haines, J.; Léger, J. M. X-Ray Diffraction Study of TiO_2 up to 49 GPa. *Phys. B* **1993**, *192*, 233−237.

(33) Arlt, T.; Bermejo, M.; Blanco, M.; Gerward, L.; Jiang, J. Z.; Staun Olsen, J.; Recio, J. M. High-Pressure Polymorphs of Anatase TiO_2. *Phys. Rev. B: Condens. Matter Mater. Phys.* **2000**, *61*, 14414−14419.

(34) Wang, J.; Hanzawa, K.; Hiramatsu, H.; Kim, J.; Umezawa, N.; Iwanaka, K.; Tada, T.; Hosono, H. Exploration of Stable Strontium Phosphide-Based Electrides: Theoretical Structure Prediction and Experimental Validation. *J. Am. Chem. Soc.* **2017**, *139*, 15668−15680.
(35) Oganov, A. R.; Pickard, C. J.; Zhu, Q.; Needs, R. J. Structure Prediction Drives Materials Discovery. *Nat. Rev. Mater.* **2019**, *4*, 331−348.
(36) Glass, C. W.; Oganov, A. R.; Hansen, N. USPEX - Evolutionary Crystal Structure Prediction. *Comput. Phys. Commun.* **2006**, *175*, 713−720.
(37) Oganov, A. R.; Glass, C. W. Crystal Structure Prediction Using Ab Initio Evolutionary Techniques: Principles and Applications. *J. Chem. Phys.* **2006**, *124*, 244704.
(38) Oganov, A. R.; Lyakhov, A. O.; Valle, M. How Evolutionary Crystal Structure Prediction Works—and Why. *Acc. Chem. Res.* **2011**, *44*, 227−237.
(39) Lyakhov, A. O.; Oganov, A. R.; Stokes, H. T.; Zhu, Q. New Developments in Evolutionary Structure Prediction Algorithm USPEX. *Comput. Phys. Commun.* **2013**, *184*, 1172−1182.
(40) Jain, A.; Ong, S. P.; Hautier, G.; Chen, W.; Richards, W. D.; Dacek, S.; Cholia, S.; Gunter, D.; Skinner, D.; Ceder, G.; et al. Commentary: The Materials Project: A Materials Genome Approach to Accelerating Materials Innovation. *APL Mater.* **2013**, *1*, 011002.
(41) Liu, Y.; Oganov, A. R.; Wang, S.; Zhu, Q.; Dong, X.; Kresse, G. Prediction of New Thermodynamically Stable Aluminum Oxides. *Sci. Rep.* **2015**, *5*, 9518.
(42) Hanaor, D. A. H.; Sorrell, C. C. Review of the Anatase to Rutile Phase Transformation. *J. Mater. Sci.* **2011**, *46*, 855−874.
(43) Marchand, R.; Brohan, L.; Tournoux, M. TiO_2 (B) a New Form of Titanium Dioxide and the Potassium Octatitanate $K_2Ti_8O_{17}$. *Mater. Res. Bull.* **1980**, *15*, 1129−1133.
(44) Banfield, J. F.; Veblen, D. R.; Smith, D. J. The Identification of Naturally Occurring TiO_2 (B) by Structure Determination Using High-Resolution Electron Microscopy, Image Simulation, and Distance-Least-Squares Refinement. *Am. Mineral.* **1991**, *76*, 343−353.
(45) Kim, K. B.; Kikuchi, M.; Miyakawa, M.; Yanagi, H.; Kamiya, T.; Hirano, M.; Hosono, H. Photoelectron Spectroscopic Study of C12A7:e^- and Alq_3 Interface: The Formation of a Low Electron-Injection Barrier. *J. Phys. Chem. C* **2007**, *111*, 8403−8406.
(46) Kitano, M.; Kanbara, S.; Inoue, Y.; Kuganathan, N.; Sushko, P. V.; Yokoyama, T.; Hara, M.; Hosono, H. Electride Support Boosts Nitrogen Dissociation over Ruthenium Catalyst and Shifts the Bottleneck in Ammonia Synthesis. *Nat. Commun.* **2015**, *6*, 6731.
(47) Kitano, M.; Inoue, Y.; Yamazaki, Y.; Hayashi, F.; Kanbara, S.; Matsuishi, S.; Yokoyama, T.; Kim, S.-W.; Hara, M.; Hosono, H. Ammonia Synthesis Using a Stable Electride as an Electron Donor and Reversible Hydrogen Store. *Nat. Chem.* **2012**, *4*, 934−940.
(48) Dong, S.; Zhao, H. Pressure-Induced Sp Ferromagnetism in Electride-Like Elemental Potassium from First-Principles. *Phys. Status Solidi B* **2014**, *251*, 527−532.
(49) Tse, J. S. A. Chemical Perspective on High Pressure Crystal Structures and Properties. *Natl. Sci. Rev.* **2020**, *7*, 149−169.
(50) Kresse, G.; Furthmüller, J. Efficient Iterative Schemes for Ab Initio Total-Energy Calculations Using a Plane-Wave Basis Set. *Phys. Rev. B: Condens. Matter Mater. Phys.* **1996**, *54*, 11169−11186.
(51) Wang, J.; Umezawa, N.; Hosono, H. Mixed Valence Tin Oxides as Novel van der Waals Materials: Theoretical Predictions and Potential Applications. *Adv. Energy Mater.* **2016**, *6*, 1501190.
(52) Wang, J.; Hao, D.; Ye, J.; Umezawa, N. Determination of Crystal Structure of Graphitic Carbon Nitride: Ab Initio Evolutionary Search and Experimental Validation. *Chem. Mater.* **2017**, *29*, 2694−2707.
(53) Wang, J.; Ye, T.-N.; Gong, Y.; Wu, J.; Miao, N.; Tada, T.; Hosono, H. Discovery of Hexagonal Ternary Phase Ti_2InB_2 and its Evolution to Layered Boride TiB. *Nat. Commun.* **2019**, *10*, 2284.
(54) Miao, N.; Wang, J.; Gong, Y.; Wu, J.; Niu, H.; Wang, S.; Li, K.; Oganov, A. R.; Tada, T.; Hosono, H. Computational Prediction of Boron-Based MAX Phases and MXene Derivatives. *Chem. Mater.* **2020**, *32*, 6947−6957.
(55) Zhang, W.; Oganov, A. R.; Zhu, Q.; Lobanov, S. S.; Stavrou, E.; Goncharov, A. F. Stability of Numerous Novel Potassium Chlorides at High Pressure. *Sci. Rep.* **2016**, *6*, 26265.
(56) Li, K.; Wang, J.; Blatov, V. A.; Gong, Y.; Umezawa, N.; Tada, T.; Hosono, H.; Oganov, A. R. Crystal and Electronic Structure Engineering of Tin Monoxide by External Pressure. *J. Adv. Ceram.* **2021**, *10*, 565−577.
(57) Blöchl, P. E. Projector Augmented-Wave Method. *Phys. Rev. B: Condens. Matter Mater. Phys.* **1994**, *50*, 17953−17979.
(58) Perdew, J. P.; Burke, K.; Ernzerhof, M. Generalized Gradient Approximation Made Simple. *Phys. Rev. Lett.* **1996**, *77*, 3865−3868.
(59) Togo, A.; Oba, F.; Tanaka, I. First-principles Calculations of the Ferroelastic Transition Between Rutile-type and $CaCl_2$-type SiO_2 at High Pressures. *Phys. Rev. B: Condens. Matter Mater. Phys.* **2008**, *78*, 134106.
(60) Tang, W.; Sanville, E.; Henkelman, G. A Grid-Based Bader Analysis Algorithm without Lattice Bias. *J. Phys.: Condens. Matter* **2009**, *21*, 084204.
(61) Maintz, S.; Deringer, V. L.; Tchougréeff, A. L.; Dronskowski, R. LOBSTER: A Tool to Extract Chemical Bonding from Plane-Wave Based DFT. *J. Comput. Chem.* **2016**, *37*, 1030−1035.

https://doi.org/10.1021/acs.jpclett.1c01133
J. Phys. Chem. Lett. 2021, 12, 5486−5493